Dopant-free twinning superlattice formation in InSb and InP nanowires

Xiaoming Yuan[1,2*], Yanan Guo[2], Philippe Caroff[2,3]*, Jun He[1], Hark Hoe Tan[2], Chennupati Jagadish[2]

1 School of Physics and Electronics, Hunan Key Laboratory for Supermicrostructure and ultrafast Process, Central South University, 932 South Lushan Road, Changsha, Hunan 410083, P. R. China

2 Department of Electronic Materials Engineering, Research School of Physics & Engineering, The Australian National University, Canberra, ACT 2601, Australia.

3 Currently at Department of Physics and Astronomy, Cardiff University, Queens Building, The Parade, Cardiff CF24 3AA, UK

* Corresponding authors: xiaoming.yuan@csu.edu.cn; CaroffP@cardiff.ac.uk

Abstract: Periodic arrangement of twin planes create a controllable polytype that can affect both the electronic and optical properties of nanowires. The approach that is most used for inducing twinning superlattice (TSL) formation in III-V nanowires is introducing impurity dopants during growth. Here, we demonstrate that controlling the growth parameters is sufficient to produce regular twinning planes in Au-catalysed InSb and InP nanowires. Our results show that TSL formation in InSb nanowires only exists in a very narrow growth window. We suggest that growth conditions induce a high concentration of In (or Sb) in the Au droplet, which plays a similar role to that of surfactant impurities such as Zn, and increase the droplet wetting angle to a spatial geometry that is favourable for TSL formation. The demonstration of TSL structure in InSb and InP nanowires by controlling the input of In (or Sb) with low surface energy further enhances fundamental understanding of TSL formation in III-V nanowires and allows us to tune the properties of these nanowires by crystal phase engineering.

1. Introduction

III-V semiconductor nanowires attract extensive interests in both applied science such as solar cell[1], photodetector[2], light emitting diode (LED)[3], field effect transistor (FET)[4] and nanowire laser[5] and fundamental science, in particular in the quest for new pseudo-particles like Majorana fermions[6, 7], interesting for topological quantum computing[8-10]. This wide range of applications stems from their size, rod-like

geometry and other advantages over their planar counterparts, including but not limited to, easy formation of different types of strained heterostructures[11], wider range of accessible bandgaps[12], straightforward integration on the silicon platform[13] and unique optical/ electrical properties[14]. One of the fascinating aspects of III-V semiconductor nanowires is the accessible and controllable polytypism of their crystal structures[15]. The only reported crystal structure in planar III-As and III-P compounds had been zinc blende (ZB) until the emergence of nanowires about a decade ago. Since then, the concept of crystal phase control has been commonly used to optimize the properties of III-V nanowires such as reducing the density of crystal defects and tuning the crystal structure between ZB and wurtzite (WZ)[16-18]. Periodic twinning, also known as twinning superlattice (TSL) in III-V nanowires is such a unique case, where the crystal structure of nanowires is pure ZB except for periodic rotational twins along nanowire growth direction of [111]B. The band structure of TSL nanowires has been predicted to adopt electronic mini-band structures[19-24]. Moreover, TSL has been reported to increase phonon scattering and reduce thermal conductivity, increasing the thermoelectric figure of merit (ZT) of nanowires[25-27]. Thus, TSL is a desired structure for thermoelectric applications. Currently, TSL has been reported in many III-As and III-P nanowires, which include InAs[28, 29], InP[30, 31], GaAs[32] and GaP[33] nanowires, as well as some Zn containing compound nanowires, such as ZnO[34], ZnSe[35], ZnS[36], ZnTe[37].

There are two approaches to induce TSL in III-V nanowires. The first one is to introduce Zn as dopant during vapour-liquid-solid (VLS) growth of the nanowires, which was first explored by Algra *et al.* showcasing the growth of Zn-doped TSL InP nanowires[31]. With the addition of Zn dopants, the nanowire surface energy becomes a dominant factor in the growth kinetics. First, the growth conditions for nanowire are favourable for the formation of {111}A and {111}B side facets. During the facet-conserving growth, the contact angle between the metal nanoparticle and the nanowire at one side of the nanowire increases and decreases at the opposite side, thus distorting the spatial configuration of the metal droplet. With continuing growth, the droplet-nanowire interface changes its shape from hexagonal to triangle-like. When the droplet is highly

distorted, it becomes energetically favourable to generate a rotational twinning plane which then allows the interface to evolve back to hexagonal-like shape. A few other reports using such approach by employing Zn dopant have shown TSL formation in GaAs, GaP and InP nanowires [31-33]. There are currently two explanations for the role of Zn during TSL formation in III-V nanowires. First, Algra et. al. proposed that the addition of Zn mainly affects the Au-nanowire interface, thereby reducing the solid-liquid interface energy difference between the ZB and WZ structure[31]. Later, Wallentin *et al.* showed that Zn can increase the ratio between the liquid-solid (γ_{LS}) and liquid-vapor (γ_{LV}) surface energies based on the observation that the contact angle between Au particle and nanowire increased with increasing addition of Zn[38]. In the formation of TSL in Zn-doped GaP nanowires, the change in γ_{LV} is three times larger than that of supersaturation (μ_{Ga}) under increasing Ga partial pressure[33], agreeing well with recent observations that surface energy plays a significant role in determining the nanowire structure[39, 40].

The second approach is by adjusting the growth parameters (i.e. temperature, V/III, nanowire diameter and etc), which has been reported in In-V nanowires, such as Au-seeded InAs nanowires[29], self-seeded InAs nanowires[28] and InP nanowires under high growth temperatures and *in-situ* HCl etching[30]. By assuming the idea that the role of Zn during TSL formation is mainly to alter the surface energy balance at the droplet, adjusting only the growth parameters for In-V and III-Sb nanowires should, in principle, enable the formation of a TSL structure, since both In and Sb have lower surface energy than Zn. Until now, no TSL III-Sb nanowires have ever been reported due to their strong preference to form twin-free ZB structure[41], though they would be excellent candidates for thermoelectric applications, thanks to a combined high intrinsic ZT value and the additional benefit of controllable surface roughness for increased phonon scattering[42]. Here, we report the first successful synthesis of TSL InSb nanowires by increasing the total flow of the precursors. We show that the formation of TSL is mainly governed by surface energy around the growth front instead of supersaturation condition within the catalyst droplet. From this understanding, we extend controlled formation of TSL in

InP nanowires solely by tuning the growth parameters.

2 Methods

Nanowires were grown in a horizontal flow metalorganic vapor phase epitaxy reactor (MOVPE, Aixtron 200/4) at 100 mbar with a total gas flow rate of 15 litres per minute. Trimethylindium (TMIn), trimethylantimony (TMSb), arsine (AsH_3) and phosphine (PH_3) were used as precursor for In, Sb, As and P, respectively. Au colloids with a diameter of 60 nm were first deposited on poly-L-lysine (PLL) treated InAs(111)B and InP(111)B substrates[43]. After Au functionalization, Au-seeded InAs and InP nanowire stems were first grown in separate runs and kept in an oxygen-free glove box connected to the growth reactor. The growth time of InAs and InP stems were adjusted to reach a length around 1 micron. Then, the grown InAs and InP nanowire stems were loaded into the reactor and heated to InSb nanowire growth temperature under AsH_3 flow. InSb nanowire growth was initiated by switching on TMIn and TMSb flows while turning off the AsH_3 supply. The standard conditions for InSb nanowires with TSL structure were as follows: the growth temperature, flow rate of TMIn and V/III ratio were fixed as 460 °C, 1.2×10^{-5} mol/min and 7, respectively.

For InP TSL nanowires, growth was performed by a two-temperature growth approach on InP (111)B substrates. First, nanowires were nucleated at 450 °C for 5 min. Then the temperature was ramped up rapidly to 600 ºC. Then nanowires were grown at this temperature for 20 min. The TMIn flow rate and V/III ratio were 0.8×10^{-5} mol/min and 1116, respectively. Au nanoparticles with a diameter of 30 nm were used for InP nanowire growth.

The morphology and crystal structure of the nanowires were examined by field emission scanning electron microscopy (SEM, Zeiss Ultraplus) and scanning transmission electron microscopy (STEM, JEOL2100F) operated at 200 kV.

3 Results and discussion

3.1 Formation of TSL in InSb nanowires

Figure 1 presents the morphology and structure of InSb nanowires using the growth conditions mentioned in the experimental section. The main body (except for the

bottom and tip) of the InSb nanowires shows taper-free morphology, with the diameter (measured around 447 nm) being much larger than that of the Au catalyst due to significant lateral growth that is commonly observed in antimonide nanowires[44, 45]. In comparison to InSb nanowires, the diameter of InAs stems underneath is very small due to the slow decomposition during the InSb growth at 460 °C without AsH_3 protection[45]. In some cases, the InAs stems are too thin to mechanically support the InSb nanowires above. Thus some InSb nanowires collapse and merge with each other during growth, which is similar to the previous report[46]. Closer observation of the nanowire morphology reveals a periodic zigzag sidewall facets (as highlighted by the white arrow in Figure 1b) indicating the formation of TSL. The periodic rotational twinning was then confirmed by bright field TEM images (Figure 1c-d) with a periodicity measured around 35±1.5 nm, demonstrating TSL formation in antimonide nanowires for the first time. The {111}A and {111}B side facets that are normally observed in TSL nanowires[31] are not observed here. InSb nanowires show predominantly flat {110} facets due to the faster growth rate in [111]A and [111]B directions, since {110} are the most stable facets for InSb[44, 45, 47-49]. The observation of TSL formation in InSb nanowires is quite surprising and interesting for the following reasons. First, this is the first demonstration of TSL structure in III-Sb nanowires. Metal seeded growth of GaSb and InSb nanowires usually adopt a ZB twin-free structure[44, 45, 47-49]. Until now, even though WZ polytype and TSL are common in InAs, InP, GaP and GaAs nanowires, rotational twins are rarely observed in GaSb nanowires. Only a few twin defects and WZ segments have been reported in InSb nanowires, with either extreme growth conditions or for self-seeded growth conditions [41, 50]. The realization of TSL structure in InSb nanowires points towards the possibility and ability to control the phase of antimonide nanowires and their effective surface roughness. Secondly, introducing Zn dopant has been the most common approach to trigger TSL in III-V nanowires, but the presence of impurity affects the electrical properties concomitantly. Controlling the crystal polytype by tuning growth parameters only is then the desired approach. It is interesting to note that the periodical twinning does not occur at the

beginning of InSb nanowire growth. Indeed, InSb nanowires first form a twin-free ZB segment with around 420 nm in length. Actually, InSb nanowires grown for 30 min just start to show the formation of periodical twinning (see Figure S1c in the supporting information). It appears that TSL formation in InSb nanowires is affected by nanowire length, since the crystal polytype switches back to ZB at the nanowire top. As InSb nanowire nucleates on the InAs nanowire stem, In and Sb contents in the Au seed can increase due to the sidewall diffusion into the catalyst, since both In and Sb adatoms (especially for In) have large diffusion length on the nanowire sidewalls[45, 51]. Such a variation between ZB and TSL has been observed in InAs nanowires with a reverse order, which is ascribed to the same fundamental growth mechanism[52]. As the In and Sb content in the Au particle increases, the spatial geometry of droplet evolves to favour the formation of periodical twinning planes instead of a ZB twin-free structure. Thus, it is assumed that status of the Au droplet, including its constituents and geometry, is a key factor in determining TSL formation.

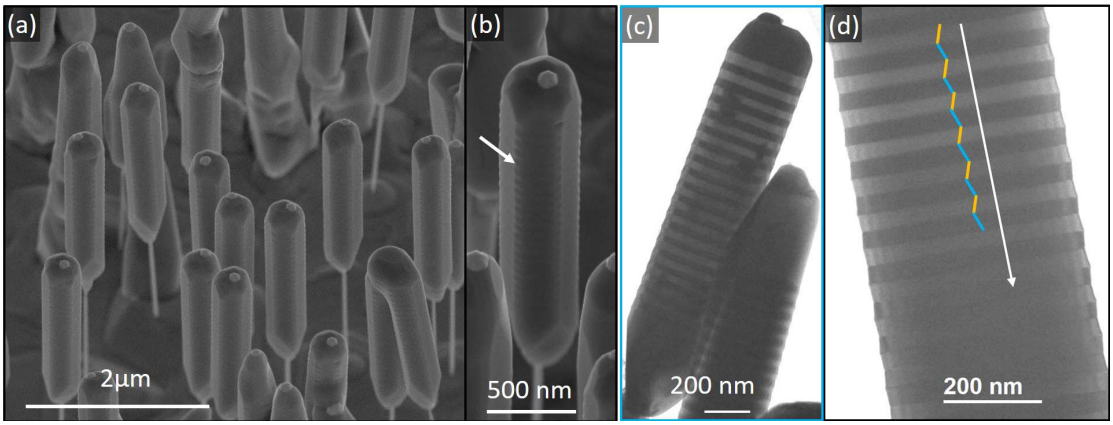

Figure 1: Formation of TSL structure in InSb nanowires. (a) 45° tilted SEM image shows the morphology with a magnified image in (b) pointing out the zigzag morphology caused by periodic twinning planes. (c-d) TEM images of the nanowires along the [1-10] zone axis, demonstrating the TSL structure. The white arrow in (d) indicates the growth direction of the nanowires.

A more detailed exploration of the parameter space was carried out to study the regime in which TSL formation is favoured in InSb nanowires. We studied the role of total

precursor flow (under constant V/III ratio) on InSb nanowire growth and the results are shown in Figure 2. When the TMIn molar flow is halved (0.6×10^{-5} mol/min) in comparison to the 'standard conditions' for TSL formation, high quality and high yield of InSb nanowires on InAs nanowire stems are achieved (Figure2 a). Moreover, lateral growth is reduced to the minimum among all the investigated growth parameters. Morphology comparison in Figure 2 demonstrates that InSb nanowire growth is strongly affected by local growth conditions. Slightly higher precursor flow leads to a drastic change in the morphology of some InSb nanowires (Figure 2b). The crystal structure evolves from ZB in Figure 2a to TSL in Figure 2c after the precursor flow is doubled. Further increase of the material supply results in a completely different morphology of the InSb nanowires (Figure 2d).

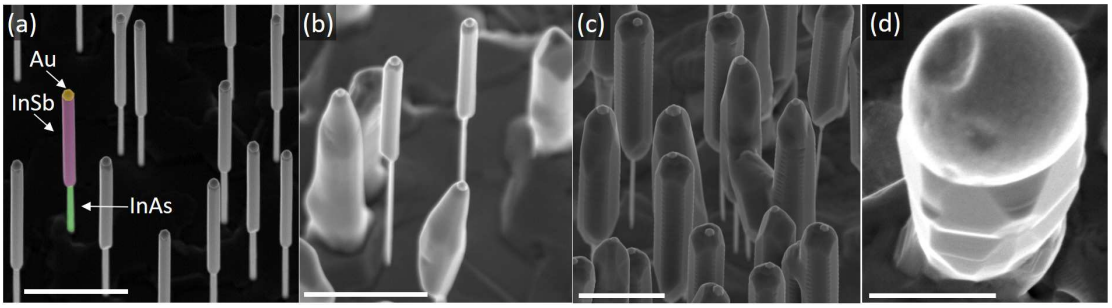

Figure 2: Role of total precursor flow on TSL formation in InSb nanowires. (a) TMIn=0.6×10^{-5} mol/min; (b) TMIn=0.9×10^{-5} mol/min; (c) TMIn=1.2×10^{-5} mol/min; (d) TMIn=1.8×10^{-5} mol/min. Growth temperature and V/III ratio are 460 °C and 7. Scale bars are 1 µm in (a-c) and 300 nm in (d)

InSb nanowires were grown on both InAs and InP stems in the same run to study the influence of the stem on InSb nanowire growth. When growing on InP stems (see Figure S2a-b), InSb nanosails are observed in addition to nanowires. In comparison, only nanowires are formed if InAs stems are used (see Figure 2a). Nanosails are formed due to an Au de-wetting process at the beginning of nanowire growth[53] favouring the formation of a single inclined twin plane driving the shape transformation, which suggests that the surface/interface energy difference of the InAs and InP nanowire stems drives the morphology difference of the InSb nanowires. These results further validate

the argument that InSb nanowire growth is very sensitive to the local growth conditions, mainly related to the composition and geometry of the Au droplet. InSb nanowires grown on InP stems also present a TSL structure (growth conditions are the same as the nanowires in Figure 2c grown on InAs stems, See Figure S2c in the supporting information), implying that the nature of the stems does not play a major role in determining the crystal phase purity in InSb nanowires. TSL formation induced by a change in total precursor flow in InSb nanowires is unexpected. Joyce *et al.* observed phase perfection in ZB structure in GaAs nanowires with an increase in material supply[54] and the current thermodynamic model for TSL formation requires a lower supersaturation[31] . By varying the total precursor flow in this work, it is found that a higher precursor supply does not result in faster axial growth rate but only increases lateral growth, which implies that supersaturation ($\Delta\mu$) in the Au droplet does not increase significantly. Again, this observation supports the validity of the argument that $\Delta\mu$ increases slowly with increasing material supply[33]. Instead, a large supply of TMIn and TMSb could reduce γ_{LV} or the ratio of γ_{LV}/γ_{LS}, which is a suitable condition for periodic twinning formation[38]. Further reducing of $\Delta\gamma_{LV}$ under too large precursor flows unpins the Au droplet at the growth front, leading to a failure of growth of InSb nanowires. These results imply that surface energy or a modified droplet contact angle (shape) critically affect the nanowire polytypism[40].

The effect of V/III ratio under constant TMIn precursor flow was also investigated to study the effect of TMSb supply on TSL formation, as shown in Figure 3. Reducing or increasing the TMSb flow from the 'standard' value of V/III ratio of 7 results in InSb nanowires with very different morphologies. When increasing the V/III ratio to 12 (Figure 3c), only a few nanowires manage to grow vertically and present a zigzag morphology, implying the presence of periodic twinning planes, as shown in the inset. Again, the TSL structure only forms after around several hundreds of nanometers. A reduction in the surface energy due to higher Sb or/and In contents in the Au droplet could tune it into an unstable shape, leading to the failure growth of vertical nanowires. With just a small change of V/III ratio, total material supply or growth temperature (see Figure S1a-b), one can modify the status of the Au seeds, resulting in unwanted InSb

nanowire growth.

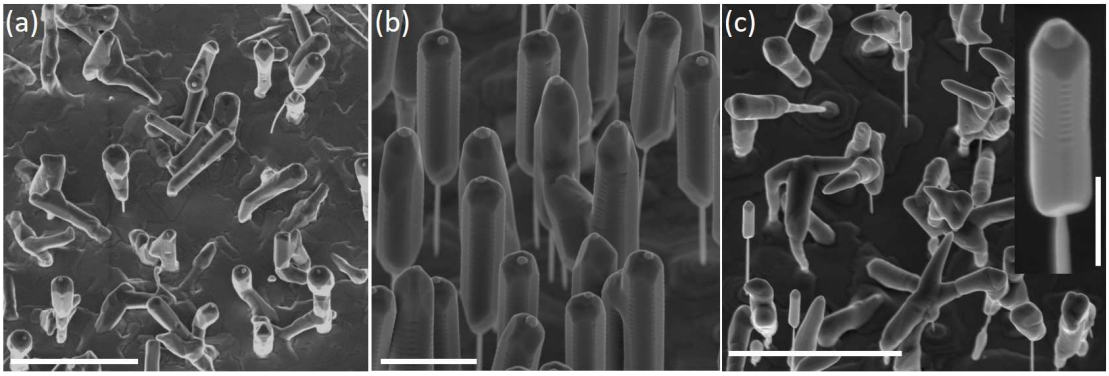

Figure 3: SEM images show that TSL formation in InSb nanowires is very sensitive to V/III ratio. (a) V/III=5 (b) V/III=7 (c) V/III=12. Inset in (c) shows one nanowire with TSL structure. Scale bars are 3 μm in (a) and (c), 1 μm in (b), and 300 nm for the inset in (c).

Introducing Zn during the nanowire growth is commonly used to engineer the effective surface roughness of nanowires, by producing periodic twinning in GaP, InP and GaAs nanowires[31-33]. However, this is not the only approach for TSL formation, since both In and Sb also have low surface energy and can be used for tuning the surface energy [39, 43, 55]. As a result, by carefully adjusting growth parameters it should, in principle, be possible to obtain TSL structure in In-related (InAs, InP) and Sb-related (GaSb and InSb) III-V nanowires. As our results show above, the crystal polytype of InSb nanowires evolves from twin-free ZB to periodic twinning by doubling the total material supply. However, this TSL only occurs within a narrow growth condition window. This could be one of the reasons why InSb TSL has not been reported, though high quality InSb nanowires were demonstrated a decade ago[44]. From our studies, TSL formation shows a strong relationship with the fraction of the constituent elements and surface energy of the Au seeds.

3.2 Taper-free InP nanowires with twinning superlattice structure

The above results show the possibility to form periodic twinning in III-V nanowires by carefully adjusting the growth parameters. Following the study of InSb nanowires, we obtained tapered-free InP nanowires with TSL via this approach. Growth conditions mentioned in the method section are designed to increase the In content and wetting

angle of the Au droplet which is expected to form ZB or TSL structures[40]. InP nanowires grown under this growth condition show taper-free morphology as demonstrated in Figure 4a. Tapering is a common issue during InP nanowire growth. For phase perfection purpose, *in-situ* HCl etching was developed to obtain InP nanowires with WZ or TSL structures[30]. Here, we show even when InP nanowires are grown at 600 °C, no tapering is observed without an etching process. Moreover, these nanowires present mostly a ZB phase with periodical twinning plane (See Figure 4c and 4d), further proving our assumption that adjusting only the growth conditions is possible for TSL formation in InP nanowires. Indeed, this is the highest level of crystal structure purity that can be achieved by changing growth parameters, since InP nanowires with pure ZB twin-free structure has never been reported before. The length of the ZB phase between the twin boundaries is around 27.6±1.9 nm. Unlike InSb nanowires, the effect of nanowire length on TSL formation is not observed in InP nanowires and the periodic twinning planes exist along the whole nanowire. Moreover, TSL can be obtained over a large range of growth parameters, such as changing the V/III ratio (realized by changing the TMIn flow) from 667 to 1117. High resolution TEM image reveals 60° rotational twin and the ZB stacking sequence. The dotted red and yellow lines indicate the original {111}B and {111}A planes after twin plane formation. These planes quickly disappear due to lateral growth.

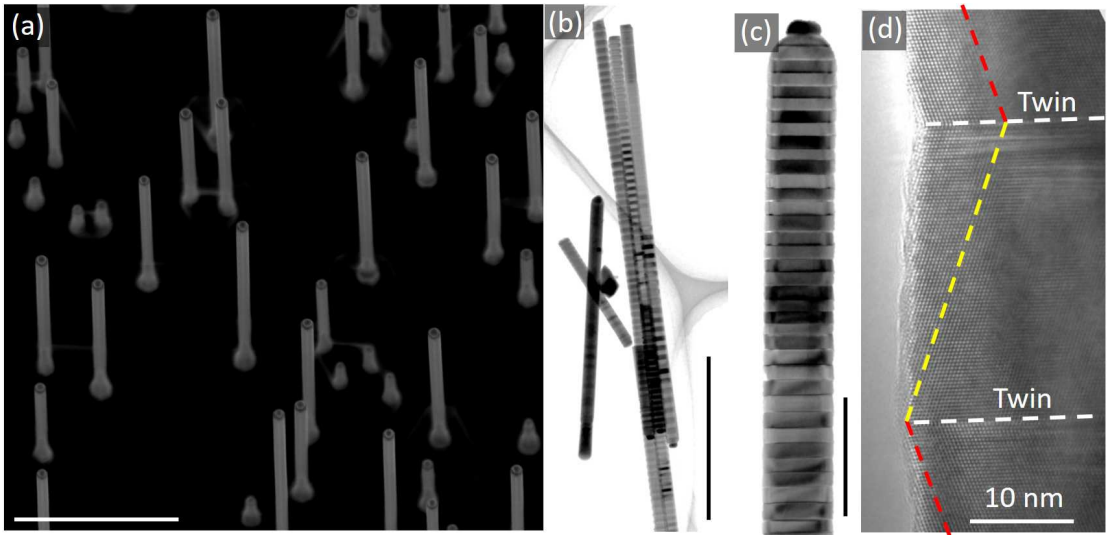

Figure 4: TSL in InP nanowires. (a) 15° tilted SEM image showing the InP nanowires

grown using a two-temperature approach. (b-c) Bright field TEM image of the nanowire in (a). (d) HRTEM image showing the twin planes. The dashed red (yellow) lines indicate {111}B ({111}A) planes. Scale bars are 1 μm in (a-b) and 200 nm in (c).

4 Conclusions

For the first time, periodic twinning superlattice formation in InSb nanowires is demonstrated. Instead of using Zn dopant, the low surface energy of In and/or Sb can be used to control the shape and contact angle of the Au particles, thus triggering TSL formation in InSb nanowires by only adjusting the growth parameters. High quality taper-free InSb nanowires with either pure ZB or TSL polytypes on InAs (or InP) nanowire stems are demonstrated. High yield of pure ZB InSb nanowires with minimal lateral growth is achieved at low precursor flow while increasing the total material supply forms a TSL structure with a segment length of around 34 nm. TSL structure in InSb nanowires is found to exist only within a very narrow growth parameter space window. Using the same approach, we show taper-free InP nanowires with TSL structure by only tuning the growth parameters. These results confirm that by adjusting the growth conditions of In-containing III-V nanowires, one can generate periodic twinning without using any impurity dopants, thereby broadening the feasibility of TSL-containing nanowires for applications in thermoelectrics.

5 Acknowledgements

The Australian Research Council (ARC) and National Natural Science Foundation of China (No. 51702368) are acknowledged for financial support. All the experimental work was performed through the Australian National Fabrication Facility, ACT Node and Australian Microscopy and Microanalysis Research Facility.

6 References

(1) Wallentin, J.; Anttu, N.; Asoli, D.; Huffman, M.; Åberg, I.; Magnusson, M. H.; Siefer, G.; Fuss-Kailuweit, P.; Dimroth, F.; Witzigmann, B.; et al. *Science* **2013**.

(2) Dai, X.; Zhang, S.; Wang, Z.; Adamo, G.; Liu, H.; Huang, Y.; Couteau, C.; Soci, C. *Nano Letters* **2014**, *14*, (5), 2688.

(3) Guo, W.; Zhang, M.; Banerjee, A.; Bhattacharya, P. *Nano Letters* **2010**, *10*, (9), 3355.

(4) Konar, A.; Mathew, J.; Nayak, K.; Bajaj, M.; Pandey, R. K.; Dhara, S.; Murali, K. V. R. M.; Deshmukh, M. M. *Nano Letters* **2015**, *15*, (3), 1684.

(5) Saxena, D.; Mokkapati, S.; Parkinson, P.; Jiang, N.; Gao, Q.; Tan, H. H.; Jagadish, C. *Nat Photon* **2013**, *7*, (12), 963.

(6) Mourik, V.; Zuo, K.; Frolov, S. M.; Plissard, S. R.; Bakkers, E. P. A. M.; Kouwenhoven, L. P. *Science* **2012**, *336*, (6084), 1003.

(7) Franz, M. *Nat Nano* **2013**, *8*, (3), 149.

(8) Nadj-Perge, S.; Frolov, S. M.; Bakkers, E. P. A. M.; Kouwenhoven, L. P. *Nature* **2010**, *468*, (7327), 1084.

(9) Hu, Y.; Kuemmeth, F.; Lieber, C. M.; Marcus, C. M. *Nat Nano* **2012**, *7*, (1), 47.

(10) Pribiag, V. S.; Nadj Perge, S.; Frolov, S. M.; van den Berg, J. W. G.; van Weperen, I.; Plissard, S. R.; Bakkers, E. P. A. M.; Kouwenhoven, L. P. *Nat Nano* **2013**, *8*, (3), 170.

(11) Dey, A. W.; Svensson, J.; Ek, M.; Lind, E.; Thelander, C.; Wernersson, L.-E. *Nano Letters* **2013**, *13*, (12), 5919.

(12) Berg, A.; Caroff, P.; Shahid, N.; Lockrey, M. N.; Yuan, X.; Borgström, M. T.; Tan, H. H.; Jagadish, C. *Nano Res.* **2017**, *10*, (2), 672.

(13) Kim, H.; Farrell, A. C.; Senanayake, P.; Lee, W.-J.; Huffaker, D. L. *Nano Letters* **2016**, *16*, (3), 1833.

(14) Joyce, H. J.; Gao, Q.; Tan, H. H.; Jagadish, C.; Kim, Y.; Zou, J.; Smith, L. M.; Jackson, H. E.; Yarrison-Rice, J. M.; Parkinson, P.; et al. *Progress in Quantum Electronics* **2011**, *35*, (2-3), 23.

(15) Caroff, P.; Bolinsson, J.; Johansson, J. *IEEE Journal of Selected Topics in Quantum Electronics* **2011**, *17*, (4), 829.

(16) Assali, S.; Zardo, I.; Plissard, S.; Kriegner, D.; Verheijen, M. A.; Bauer, G.; Meijerink, A.; Belabbes, A.; Bechstedt, F.; Haverkort, J. E. M.; et al. *Nano Letters* **2013**, *13*, (4), 1559.

(17) Vainorius, N.; Lehmann, S.; Jacobsson, D.; Samuelson, L.; Dick, K. A.; Pistol, M.-E. *Nano Letters* **2015**, *15*, (4), 2652.

(18) Assali, S.; Gagliano, L.; Oliveira, D. S.; Verheijen, M. A.; Plissard, S. R.; Feiner, L. F.; Bakkers, E. P. A. M. *Nano Letters* **2015**, *15*, (12), 8062.

(19) Ikonić, Z.; Srivastava, G. P.; Inkson, J. C. *Physical Review B* **1993**, *48*, (23), 17181.

(20) Ikonic, Z.; Srivastava, G. P.; Inkson, J. C. *Physical Review B* **1995**, *52*, (19), 14078.

(21) Tadic, M.; Ikonic, Z. *Journal of Physics: Condensed Matter* **1999**, *11*, (36), 6891.

(22) Akiyama, T.; Yamashita, T.; Nakamura, K.; Ito, T. *Nano Letters* **2010**, *10*, (11), 4614.

(23) Tsuzuki, H.; Cesar, D. F.; Rebello de Sousa Dias, M.; Castelano, L. K.; Lopez-Richard, V.; Rino, J. P.; Marques, G. E. *ACS Nano* **2011**, *5*, (7), 5519.

(24) Shimamura, K.; Yuan, Z.; Shimojo, F.; Nakano, A. *Applied Physics Letters* **2013**, *103*, (2), 022105.

(25) Moore, A. L.; Saha, S. K.; Prasher, R. S.; Shi, L. *Applied Physics Letters* **2008**, *93*, (8), 083112.

(26) Sansoz, F. *Nano Lett* **2011**, *11*, (12), 5378.

(27) Nika, D. L.; Cocemasov, A. I.; Isacova, C. I.; Balandin, A. A.; Fomin, V. M.; Schmidt, O. G. *Physical Review B* **2012**, *85*, (20), 205439.

(28) Th, G.; Rieger, T.; Ch, B.; Th, S.; Grützmacher, D.; Lepsa, M. I. *Nanotechnology* **2013**, *24*, (33), 335601.

(29) Caroff, P.; Dick, K. A.; Johansson, J.; Messing, M. E.; Deppert, K.; Samuelson, L. *Nat. Nanotechnol.* **2009**, *4*, (1), 50.

(30) Vu, T. T.; Zehender, T.; Verheijen, M. A.; Plissard, S. R.; Immink, G. W.; Haverkort, J. E.; Bakkers, E. P. *Nanotechnology* **2013**, *24*, (11), 115705.

(31) Algra, R. E.; Verheijen, M. A.; Borgstrom, M. T.; Feiner, L. F.; Immink, G.; van Enckevort, W. J.; Vlieg, E.; Bakkers, E. P. *Nature* **2008**, *456*, (7220), 369.

(32) Burgess, T.; Breuer, S.; Caroff, P.; Wong-Leung, J.; Gao, Q.; Hoe Tan, H.; Jagadish, C. *ACS Nano* **2013**, *7*, (9), 8105.

(33) Algra, R. E.; Verheijen, M. A.; Feiner, L.-F.; Immink, G. G. W.; Enckevort, W. J. P. v.; Vlieg, E.; Bakkers, E. P. A. M. *Nano Letters* **2011**, *11*, (3), 1259.

(34) Soonjae, K.; Sekwon, N.; Haseok, J.; Sunho, K.; Byunghoon, L.; Jaehyun, Y.; Hyoungsub, K.; Hoo-Jeong, L. *Nanotechnology* **2013**, *24*, (6), 065703.

(35) Li, Q.; Gong, X.; Wang, C.; Wang, J.; Ip, K.; Hark, S. *Advanced Materials* **2004**, *16*, (16), 1436.

(36) Hao, Y.; Meng, G.; Wang, Z. L.; Ye, C.; Zhang, L. *Nano Letters* **2006**, *6*, (8), 1650.

(37) Meng, Q.; Jiang, C.; Mao, S. X. *Journal of Crystal Growth* **2008**, *310*, (20), 4481.

(38) Wallentin, J.; Ek, M.; Wallenberg, L. R.; Samuelson, L.; Deppert, K.; Borgstrom, M. T. *Nano Lett* **2010**, *10*, (12), 4807.

(39) Yuan, X.; Caroff, P.; Wong-Leung, J.; Fu, L.; Tan, H. H.; Jagadish, C. *Advanced Materials* **2015**, *27*, (40), 6096.

(40) Jacobsson, D.; Panciera, F.; Tersoff, J.; Reuter, M. C.; Lehmann, S.; Hofmann, S.; Dick, K. A.; Ross, F. M. *Nature* **2016**, *531*, (7594), 317.

(41) Gorji Ghalamestani, S.; Lehmann, S.; Dick, K. A. *Nanoscale* **2016**, *8*, (5), 2778.

(42) Cheng, Y.; Yang, J.; Jiang, Q.; He, D.; He, J.; Luo, Y.; Zhang, D.; Zhou, Z.; Ren, Y.; Xin, J. *J. Mater. Chem. A* **2017**, *5*, (10), 5163.

(43) Yuan, X.; Caroff, P.; Wong-Leung, J.; Tan, H. H.; Jagadish, C. *Nanoscale* **2015**, *7*, (11), 4995.

(44) Caroff, P.; Wagner, J. B.; Dick, K. A.; Nilsson, H. A.; Jeppsson, M.; Deppert, K.; Samuelson, L.; Wallenberg, L. R.; Wernersson, L. E. *Small* **2008**, *4*, (7), 878.

(45) Plissard, S. R.; Slapak, D. R.; Verheijen, M. A.; Hocevar, M.; Immink, G. W. G.; van Weperen, I.; Nadj-Perge, S.; Frolov, S. M.; Kouwenhoven, L. P.; Bakkers, E. P. A. M. *Nano Lett* **2012**, *12*, (4), 1794.

(46) Plissard, S. R.; van Weperen, I.; Car, D.; Verheijen, M. A.; Immink, G. W. G.; Kammhuber, J.; Cornelissen, L. J.; Szombati, D. B.; Geresdi, A.; Frolov, S. M.; et al. *Nat Nano* **2013**, *8*, (11), 859.

(47) Lugani, L.; Ercolani, D.; Sorba, L.; Sibirev, N. V.; Timofeeva, M. A.; Dubrovskii, V. G. *Nanotechnology* **2012**, *23*, (9).

(48) Lugani, L.; Ercolani, D.; Rossi, F.; Salviati, G.; Beltram, F.; Sorba, L. *Cryst Growth Des* **2010**, *10*, (9), 4038.

(49) Guo, Y. N.; Zou, J.; Paladugu, M.; Wang, H.; Gao, Q.; Tan, H. H.; Jagadish, C. *Appl Phys Lett* **2006**, *89*, (23).

(50) Pozuelo, M.; Zhou, H. L.; Lin, S.; Lipman, S. A.; Goorsky, M. S.; Hicks, R. F.;

Kodambaka, S. *J Cryst Growth* **2011**, *329*, (1), 6.

(51) Madsen, M. H.; Krogstrup, P.; Johnson, E.; Venkatesan, S.; Mühlbauer, E.; Scheu, C.; Sørensen, C. B.; Nygård, J. *J Cryst Growth* **2013**, *364*, 16.

(52) Dick, K. A.; Thelander, C.; Samuelson, L.; Caroff, P. *Nano Letters* **2010**, *10*, (9), 3494.

(53) de la Mata, M.; Leturcq, R.; Plissard, S. R.; Rolland, C.; Magen, C.; Arbiol, J.; Caroff, P. *Nano Lett* **2016**, *16*, (2), 825.

(54) Joyce, H. J.; Gao, Q.; Tan, H. H.; Jagadish, C.; Kim, Y.; Fickenscher, M. A.; Perera, S.; Hoang, T. B.; Smith, L. M.; Jackson, H. E.; et al. *Nano Letters* **2009**, *9*, (2), 695.

(55) Yuan, X.; Caroff, P.; Wang, F.; Guo, Y.; Wang, Y.; Jackson, H. E.; Smith, L. M.; Tan, H. H.; Jagadish, C. *Advanced Functional Materials* **2015**, *25*, (33), 5300.

Supporting information

Dopant-free twinning superlattice formation in InSb and InP nanowires

Xiaoming Yuan[1,2*], Yanan Guo[2], Philippe Caroff[2,3]*, Jun He[1], Hark Hoe Tan[2], Chennupati Jagadish[2]

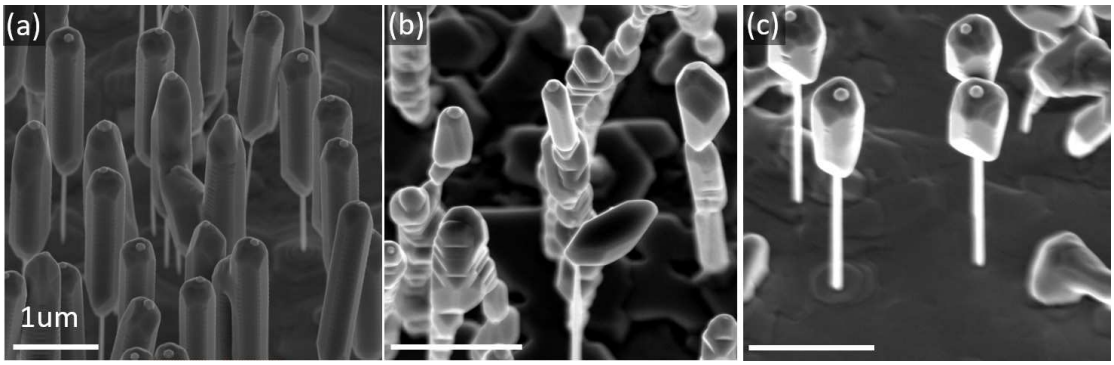

Figure S1: SEM images compare the InSb nanowire morphology grown at different conditions. (a) Nanowires grown at reference growth condition for TSL for 1h. (b) nanowires grown at 475 °C. (c) Nanowires grown at reference growth condition for TSL for 30min.

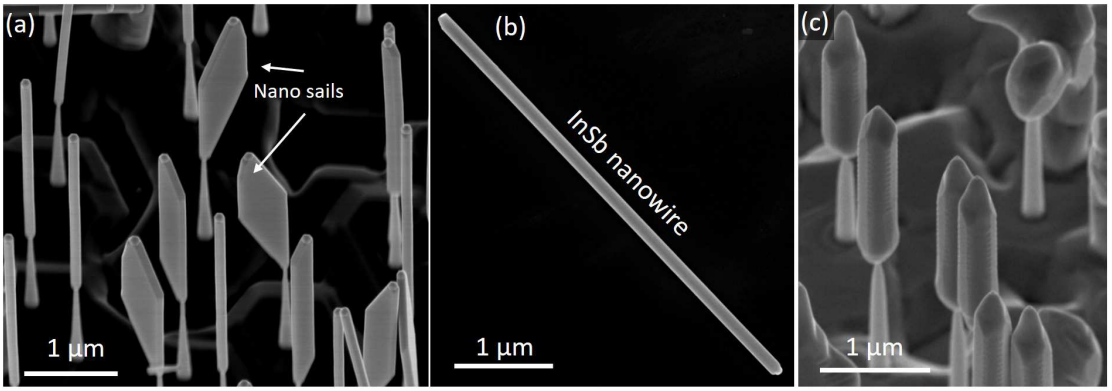

Figure S2. InSb nano-structures grown on ex-situ InP nanowire stems. (a) 30° tilted SEM image of the InSb grown with the same conditions as InSb nanowires shown in Figure 2a. InSb nano-sails are found in addition to InSb nanowires, again demonstrating that the InSb morphology sensitively dependent on the spatial configuration of the droplets. (b) Enlarged SEM image of the InSb nanowires in (a) after transferring to Si

substrate, showing the taper-free morphology with 5 μm long and 145 nm in diameter. (c) 45° titled SEM image of the InSb TSL nanowires which were grown in the same patch as InSb TSL nanowires on InAs stems in figure 1. These findings demonstrate two things. First, InSb nanowire growth can use different stems and the used stems will affect the morphology of nanowires. Secondly, TSL in InSb nanowires can also form on different nanowire stems.